ARTICLE

Guiding Brain Tumor Resection Using Surface-Enhanced Raman Scattering Nanoparticles and a Hand-Held Raman Scanner

Hazem Karabeber,[†,‡] Ruimin Huang,[†,‡,§,⊗] Pasquale Iacono,[†,‡,⊗] Jason M. Samii,[†,‡] Ken Pitter,[§,⊥] Eric C. Holland,[∥] and Moritz F. Kircher[†,‡,§,#,*]

[†]Department of Radiology, Memorial Sloan Kettering Cancer Center, New York, New York 10065, United States, [‡]Center for Molecular Imaging and Nanotechnology (CMINT), Memorial Sloan Kettering Cancer Center, New York, New York 10065, United States, [§]Brain Tumor Center, Memorial Sloan Kettering Cancer Center, New York, New York 10065, United States, [⊥]Cancer Biology and Genetics Program, Memorial Sloan Kettering Cancer Center, New York, New York 10065, United States, [∥]Human Biology and Solid Tumor Translational Research, Fred Hutchinson Cancer Research Center, Alvord Brain Tumor Center, University of Washington, Seattle, Washington 98019, United States, and [#]Department of Radiology, Weill Cornell Medical College, New York, New York 10065, United States. [⊗]These authors contributed equally to this work.

ABSTRACT The current difficulty in visualizing the true extent of malignant brain tumors during surgical resection represents one of the major reasons for the poor prognosis of brain tumor patients. Here, we evaluated the ability of a hand-held Raman scanner, guided by surface-enhanced Raman scattering (SERS) nanoparticles, to identify the microscopic tumor extent in a genetically engineered RCAS/tv-a glioblastoma mouse model. In a simulated intraoperative scenario, we tested both a static Raman imaging device and a mobile, hand-held Raman scanner. We show that SERS image-guided resection is more accurate than resection using white light visualization alone. Both methods complemented each other, and correlation with histology showed that SERS nanoparticles accurately outlined the extent of the tumors. Importantly, the hand-held Raman probe not only allowed near real-time scanning, but also detected additional microscopic foci of cancer in the resection bed that were not seen on static SERS images and would otherwise have been missed. This technology has a strong potential for clinical translation because it uses inert gold–silica SERS nanoparticles and a hand-held Raman scanner that can guide brain tumor resection in the operating room.

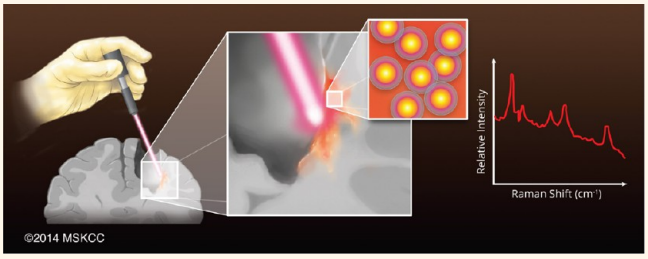

KEYWORDS: surface-enhanced Raman scattering (SERS) · SERS nanoparticles · SERS-guided tumor resection · hand-held Raman scanner · brain tumors · glioblastoma multiforme · GBM

The treatment of malignant brain tumors, in particular glioblastoma multiforme (GBM) (= WHO grade IV astrocytoma), remains one of the greatest challenges in oncology, with an average mean survival for GBM patients of only 12–15 months.[1,2] Surgery remains a mainstay in the treatment of brain tumors, because tumor resections improve patient survival[3–6] and because the extent of resection (percentage of tumor removed) of both primary and recurrent tumors directly correlates with the length of survival.[4,6–8] Most importantly, studies examining patterns of brain tumor recurrence have consistently shown that 80–90% of recurrences are within the original treatment field, indicating that the cause are residual tumor cells left behind due to incomplete tumor resections.[9,10] However, neurosurgeons are currently hindered in achieving complete resections because of indistinct tumor margins and microscopic tumor infiltrating several centimeters into the surrounding brain, which is impossible to detect with currently available methods.[11] Therefore, there is a critical unmet need for a method that enables discrimination of tumor from surrounding normal brain structures with microscopic precision in the operating room.

Among the different malignant brain tumor types, we have chosen GBM because these tumors are considered the most challenging to resect due to the diffuse pattern of tumor spread. It has been shown that the

* Address correspondence to kircherm@mskcc.org.

Received for review March 6, 2014 and accepted August 5, 2014.

Published online August 05, 2014
10.1021/nn503948b

estimate of gross tumor burden reduction by neurosurgeons is much less accurate than postoperative modern neuroimaging assessments.[12,13] Different imaging techniques are currently being utilized to better visualize tumor margins. Presurgical magnetic resonance imaging (MRI) is used to plan stereotactic surgery and determine the macroscopic outline of the tumor.[14,15] Several studies have suggested that MRI using FLAIR, diffusion-weighted and T2-weighted sequences is also able to image infiltrative microscopic tumor spread.[16,17] However, the assessment of tumor borders by preoperative MRI is often incongruent with the actual tumor borders during surgery due to brain shift during the operative procedure.[14,18] Intraoperative MRI is also limited by the necessity for frequent administrations of gadolinium (Gd)-chelates because of their short blood half-lives,[19] and by the inaccuracies of false-positive contrast enhancement.[20] Small molecule Gd-agents disperse from the initial area of tumor enhancement into the peritumoral zone of edema over time, therefore causing inaccuracies in estimating the true tumor borders.[21] Ultrasonography is being used at several centers and has been reported to improve patient outcome,[22,23] but cannot visualize microscopic cancer. Several optical methods have been suggested, either based on intrinsic tissue optical properties[11,24,25] or on exogenous contrast agents.[14,26−29] However, these optical techniques often are limited by small fields of view (microscopy), decreased specificity due to autofluorescence, or rapid photobleaching. These and other factors limit their potential to localize the true extent of the tumor in a clinical scenario.[30,31]

We have recently reported, using a static surface-enhanced Raman scattering (SERS) imaging microscope, that suitable SERS nanoparticles can serve as an image-guidance tool and help in identifying microscopic tumor in implanted glioma mouse models.[14] While real-time SERS imaging in the operating room would be highly desirable, it is not currently possible as rapid wide-field SERS imaging devices have not yet been developed. To address this limitation, we have developed an intraoperative tumor detection method that could be applied clinically in the near future. We assessed the feasibility of a novel combination of static SERS imaging and near real-time SERS nanoparticle detection using a hand-held Raman scanner, in an intraoperative scenario. This was accomplished in a genetic mouse model that closely mimics the pathology of human GBM. We found that static SERS imaging serves as an excellent image-guidance tool for tumor resection, even in this infiltrative GBM model. Importantly, we found that a hand-held Raman scanner could be used to scan, in near real-time, the resection bed for any residual microscopic tumor foci, especially in areas that could not be reached *via* static SERS imaging. Doing so, we identified microscopic foci at the resection margins that would have been missed with static SERS imaging alone. After tumor resection was completed with this method, without requiring wide safety margins, no residual GBM tumor cells were left in the resection bed as confirmed by histological methods. Given that the SERS nanoparticles used in this study have passed extensive cytotoxicity studies[32] and the hand-held Raman scanner tested here is already used in clinical trials for detection of intrinsic Raman spectra,[33] this tumor-detection method has a strong potential for clinical translation and testing.

RESULTS

Study Design. Our study included three different groups (n = 5 mice each) using different methods of brain tumor resection. We used the genetically engineered GBM mouse model (PDGF-driven gliomas using RCAS/tv-a),[34] which is known to mimic human glioblastomas very closely at a histological level.[35−37] Four weeks after RCAS-injection, mouse brains were imaged by *in vivo* T2-weighted MRI to determine tumor size and location. Fifteen GBM bearing mice were selected *via* MRI screening. All mice had tumors of similar size (diameter of 2−5 mm), and were injected with gold−silica SERS nanoparticles (Figure 1A−C) *via* tail vein (150 μL volume, 28.0 nM SERS nanoparticle concentration).

The particles were allowed to circulate for 24 h to ensure that they accumulated in the tumors. Mouse brains were then harvested, fixed in 4% paraformaldehyde, and randomly divided into 3 groups (see study design in Figure 2): (i) "Resection without Raman guidance", where tumor resection was only based on white light illumination; (ii) "Resection with guidance by Raman microscope", using static SERS imaging (Raman microscope, Figure 1D), followed by hand-held SERS scanning (Figure 1E; to confirm the completeness of resection); and (iii) "Resection with guidance by hand-held Raman scanner", where only the hand-held Raman scanner was used to guide the tumor resection. In groups (ii) and (iii), both static SERS imaging and hand-held SERS scanning were used in order to cross-validate the methods.

(i). Resection without Raman Guidance. See Supporting Information (Figure S1).

(ii). Raman Microscope Imaging-Guided Tumor Resection. The brains (n = 5) were scanned utilizing the Raman microscope (fixed 90° angle of illumination). Raman images depicted the outline of tumors (Figure 3B1), which correlated in location with the abnormality seen with white light illumination (Figure 3A1). The presence of SERS-active Raman foci was confirmed with a second scan with the Raman hand-held probe at a 90° angle, which also detected the SERS spectrum of the SERS nanoparticles at the same foci (Figure 3C1). Surgical removal of the Raman positive area on the SERS image was performed next (Figure 3A2), with acquisition of SERS images (Figure 3B2) between each resection step. The Raman positive foci detected with the

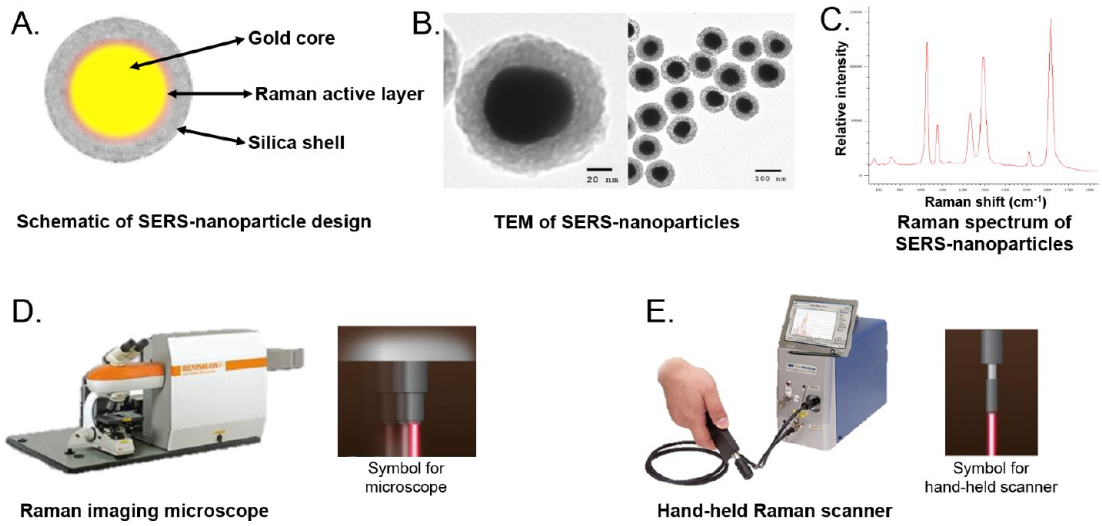

Figure 1. (A) Diagram of the SERS-nanoparticle design, depicting the gold core, Raman reporter layer (4,4′-dipyridyl), and dye-encapsulating silica shell. (B) Transmission electron microscopy images of the SERS nanoparticles. (C) Unique Raman "fingerprint" spectrum of the SERS nanoparticles (acquisition time =1s, 100 mW laser power). (D) Raman microscope used to acquire images in this study (adjacent schematic serves as the symbol for the microscope in the remaining figures). (E) Hand-held Raman scanner (adjacent schematic serves as the symbol for the microscope in the remaining figures).

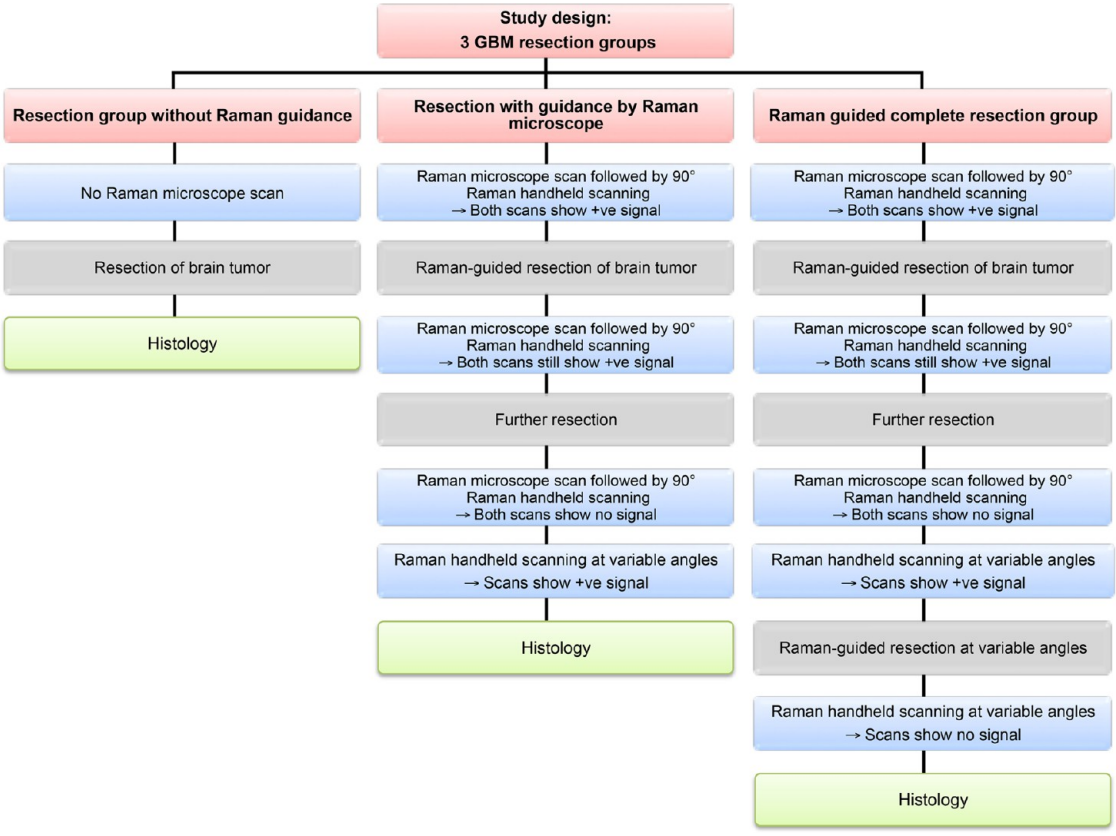

Figure 2. Flow diagram of the study design.

SERS microscope were then probed with the hand-held Raman scanner at the same 90° angle, which detected the signature of our SERS nanoparticles in the same locations (Figures 3C2). After these Raman positive foci were resected, the tumor beds were reimaged with the Raman microscope, with no residual Raman signal detected (Figure 3B3). Similar scanning with the hand-held Raman scanner at 90° angle did not reveal any SERS nanoparticle spectra either (Figure 3C3).

We hypothesized that small foci of tumor in the lateral margins of the resection bed can remain undetected if scanning is only performed using a 90°

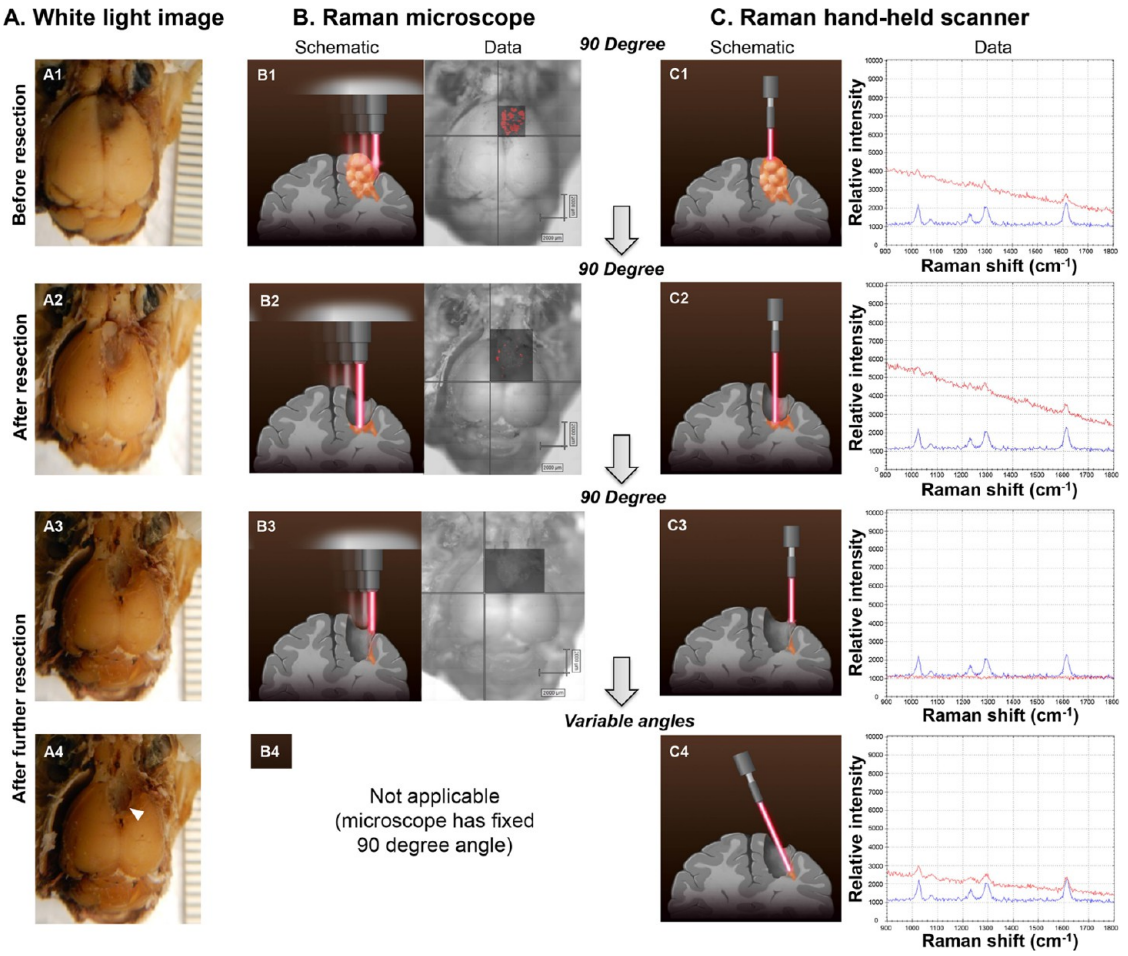

Figure 3. GBM resection with guidance by Raman microscope. (A) Photographs of the intact brain before (A1) and after (A2 and A3) successive tumor resections guided by the Raman microscope (fixed 90° angle). When the hand-held Raman scanner was used at variable angles after these resection steps, additional microscopic tumor tissue was detected (location depicted by arrowhead in A4). (B) SERS images acquired with the Raman microscope before (B1) and after (B2 and B3) successive tumor resections. (C) The hand-held Raman scanner was used for verification of signal (C1−C3) observed with the Raman microscope (B1−B3). (C4) Angulated scanning of the lateral wall of the resection bed with the hand-held Raman scanner detected microscopic tumor, which had been missed by the Raman microscope. Tissue was left in place for histological verification *in situ* (red Raman spectra = nanoparticles detected in brain tissue; blue Raman spectra = SERS nanoparticle standard as control).

angle, due to overlying normal brain tissue attenuating the laser beam (Figure 3B3,C3). We therefore proceeded to rescan the resection bed with the hand-held scanner by tilting the probe at variable angles to assess the lateral walls of the resection bed. Indeed, we observed residual Raman positive foci along the lateral margins that were previously undetected by imaging at 90° (Figure 3C4). We marked the locations of these Raman active foci without resecting them, in order to be able to histologically confirm them *in situ*. Histology demonstrated microscopic extensions of tumor into the surrounding brain tissue at these locations (Figure 4).

(iii). Hand-Held Raman Scanner-Guided Tumor Resection. Experiments were performed in the same fashion as in group (ii), except that the Raman positive foci that were detected with the hand-held Raman scanner using variable angle scanning (Figure 5C4) were surgically resected. This was followed by rescanning of the resection bed with the hand-held scanner until no residual Raman positive foci were detected (Figure 5C5). Histological processing of the resection bed revealed no residual tumor cells (Figure 6).

These experiments demonstrate that small foci of residual Raman signal can be detected with the hand-held Raman scanner that are otherwise undetectable with fixed angle SERS imaging. We conclude that this is due to the ability of the surgeon to change the Raman hand-held probe angle to reach out to detect otherwise obscured Raman positive foci in the resection bed.

Figure 7 shows a representative example of tumor tissue detected only with the hand-held scanner. The tissue that was detected with the angulated hand-held Raman scanner (Figure 7A) and subsequently resected (Figure 7B,D) demonstrated the presence of the SERS nanoparticle Raman signature (Figure 7C) that was confirmed to be tumor by transmission electron microscopy (TEM) and histology. TEM showed the presence

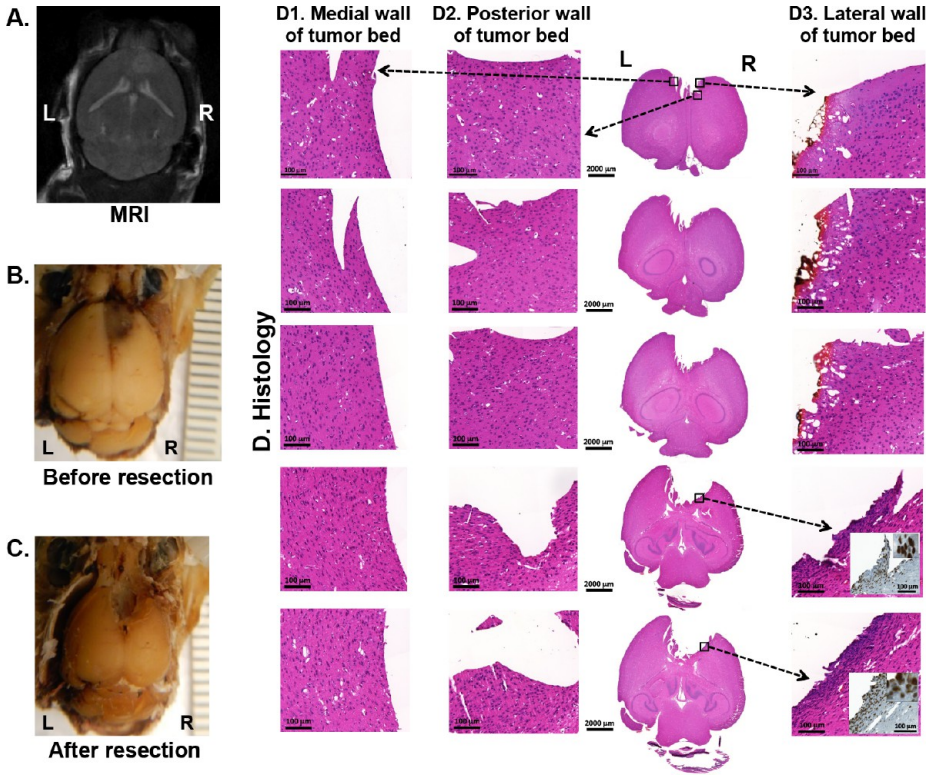

Figure 4. GBM resection with guidance by Raman microscope and histological validation. (A) T2-weighted brain MRI, showing a mass in the right frontal lobe. (B) White light photograph of the intact brain before resection, showing a discoloration in the area of the brain tumor corresponding in location to the MRI. (C) Photograph of the tumor bed after resection based on the Raman microscope images. (D) Cranial (top) to caudal (bottom) H&E stained histology images of axial brain sections after completion of surgery. D1−D3 depict healthy brain tissue on the medial (D1) and posterior (D2) walls of the resection bed, while residual tumor was present on the lateral (D3) wall of the tumor on deeper sections (insets represent immunohistochemical staining with anti-olig-2 antibody).

of SERS nanoparticles within the resected specimen (Figure 7E). H&E and immunohistochemical staining for the tumor marker Olig-2 confirmed that the resected tissue indeed represented microscopic GBM cancer spread (Figure 7F,G).

Hand-Held Raman Scanning of SERS Nanoparticles Detects Intraventricular Tumor Spread. Remarkably, in one of the mice, Raman hand-held scanning using variable angles detected SERS signal within the right lateral ventricle (Figure 8A,B). As confirmed by subsequent H&E and anti-olig-2 immunohistochemical staining, the Raman signal corresponded to a microscopic (~150−200 μm) cluster of tumor cells in the right lateral ventricle on the deepest brain sections (Figure 8C,D).

Validation and Quantification of SERS Nanoparticle Accumulation within GBM Tumors. To further validate the accumulation of the SERS nanoparticles within the GBM tumors, we performed correlation between immunohistochemical staining for tumor tissue and TEM imaging visualizing the SERS nanoparticles. This consistently showed the presence of SERS nanoparticles (black circles, corresponding to the gold core) within the tumor tissue (Figure 9A). To quantify the SERS nanoparticle uptake within tumors, we measured the gold content within tumor samples with inductively coupled plasma mass spectrometry (ICP-MS). Because the SERS nanoparticles have a gold core of defined size, this method allows quantification of intratumoral SERS nanoparticle uptake. The result was 0.8 ± 0.31% injected dose (ID) per gram tumor tissue (Figure 9B).

DISCUSSION

The detection of SERS nanoparticles with Raman spectroscopy has major advantages over other molecular contrast agent approaches such as fluorescence imaging, in that it offers not only very high sensitivity but also a unique specificity of detection. SERS nanoparticles cause massive signal amplification of an exogenous reporter built into the nanoparticle, which results in a unique Raman "fingerprint".[14,38] This overcomes disadvantages of fluorescent molecular imaging agents, where autofluorescence can often be limiting by creating false-positive signal. In delicate surgical scenarios such as brain tumor removal eliminating any unnecessary resection of healthy tissue is especially important.

Because of the diffuse pattern of GBM invasion into adjacent brain tissue, it is uncertain whether a truly complete surgical removal of all tumor cells (and therefore cure) would be feasible in humans, even with the availability of the most sensitive image-guidance technology. However, complete surgical resections are

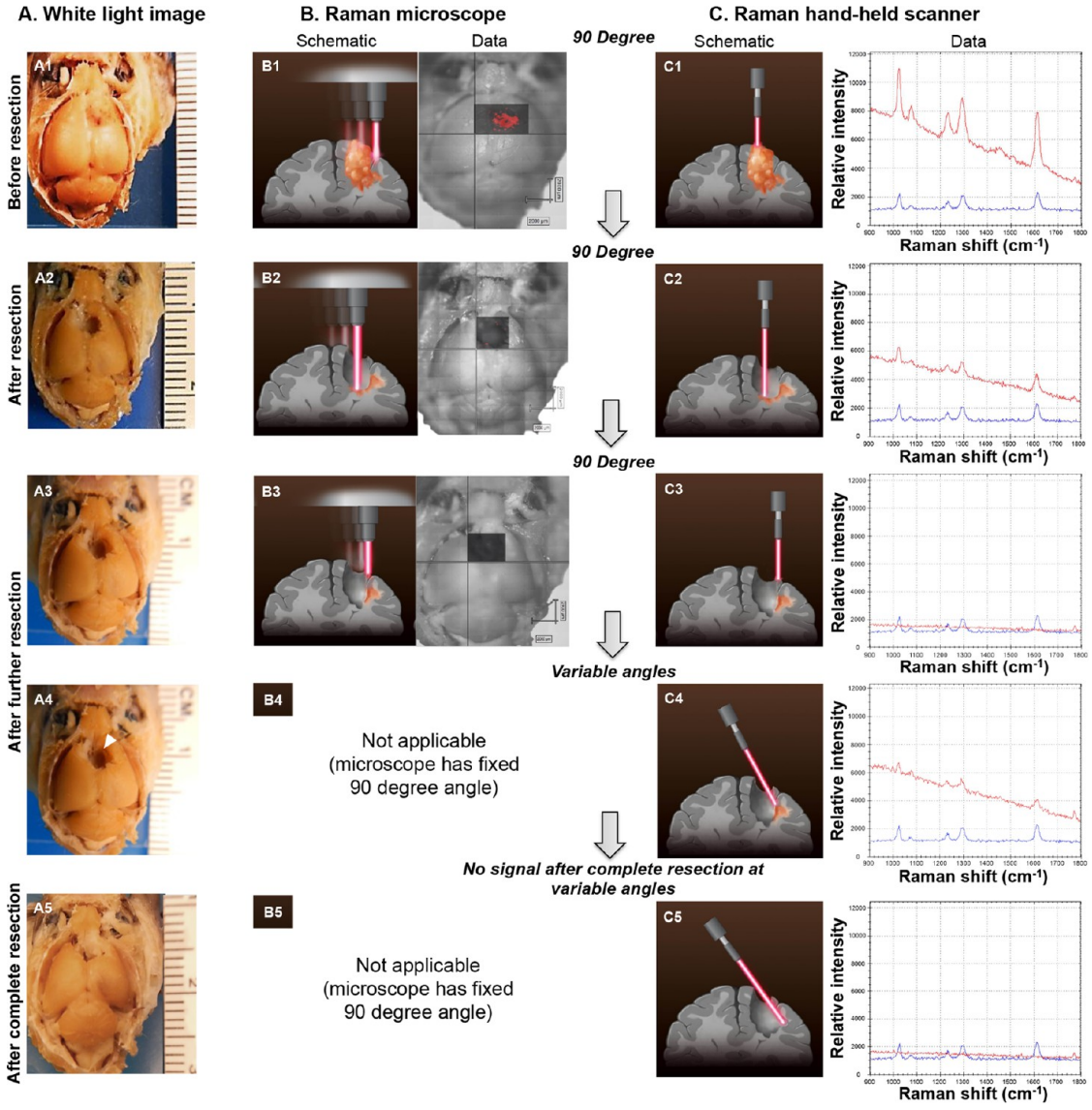

Figure 5. GBM Resection with guidance by hand-held Raman scanner. (A) Photographs of the intact brain before (A1) and after (A2 and A3) successive tumor resections guided by the hand-held Raman scanner (90° angle). When the hand-held Raman scanner was used at variable angles after these resection steps, additional microscopic tumor tissue was detected (location depicted by arrowhead in A4). (B) SERS images acquired with the Raman microscope before (B1) and after (B2 and B3) successive tumor resections. (C) Hand-held Raman scanner verified data acquired with the Raman microscope (C1−3). Angulated scanning with the hand-held Raman scanner detects microscopic tumor in the lateral wall of the tumor bed that would have been missed otherwise (C4). Additional resection was performed, and repeat angulated scanning with the hand-held scanner resulted in no detectable residual Raman signal (C5). The resection bed was then processed histologically (red Raman spectra = nanoparticles detected in brain tissue; blue Raman spectra = SERS nanoparticle standard as control).

feasible in other brain tumor types, especially those occurring in children such as, *e.g.*, ependymomas or pilocytic astrocytomas.[6,39,40] We deliberately chose a GBM model for the purpose of testing our technique in order to evaluate how well it would perform in the most extreme and difficult scenario. Given the homing mechanism of the SERS nanoparticles, which to a large part is relying on the "enhanced permeability and retention" (EPR) effect,[14] the technique should also be applicable to other brain tumor types.

We have recently shown that a previous generation of SERS nanoparticles (same dimensions but different Raman reporter as the S420 used here) is capable of detecting microscopic tumor extensions in GBM mouse models using orthotopic implantation of tumor cells (U87MG and TS543).[14] However, these models do not faithfully recapitulate human tumors. Thus, there is the need to evaluate whether such nanoparticles also work in animal models that more closely mimic human GBM tumors, such as the genetically engineered RCAS-PDGF-driven/tv-a[34] murine model used in this study.

Although SERS images acquired with a Raman microscope are promising in detecting microscopic GBM infiltrations, SERS imaging using a Raman microscope is currently not a real-time imaging method; imaging requires acquisition times in the order of minutes to

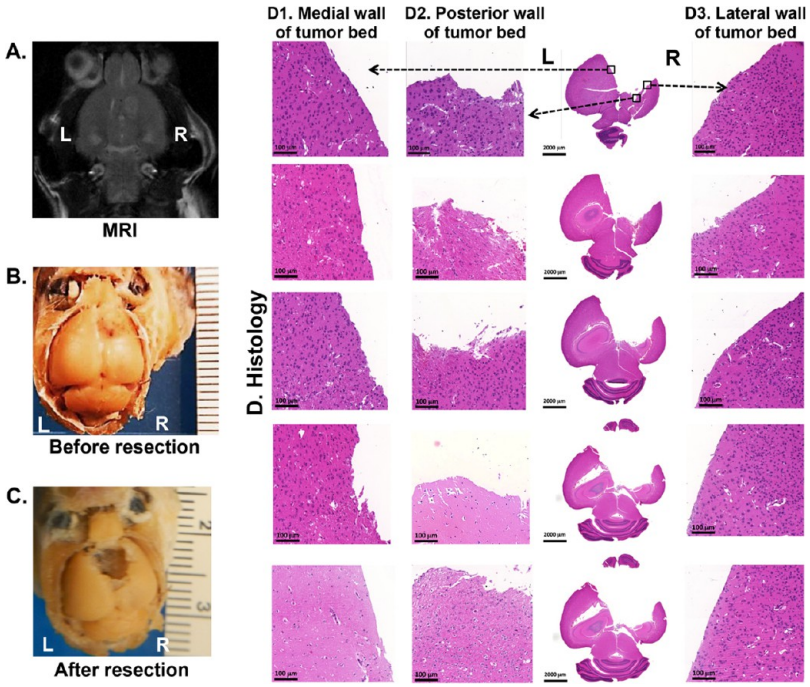

Figure 6. GBM resection with guidance by the hand-held Raman scanner and histological validation. (A) T2-weighted brain MRI, showing a mass in the right frontal lobe. (B) White light photograph of the intact brain before resection, showing a discoloration in the area of the brain corresponding in location to the MRI image. (C) Photograph of the tumor bed after SERS nanoparticle-guided resection. (D) Cranial (top) to caudal (bottom) H&E stained histological images of axial brain sections after completion of surgery. D1−D3 depict healthy brain tissue on the medial (D1), posterior (D2), and lateral (D3) walls of exposed tumor bed postresection, with no residual tumor cells detected.

hours, depending on the desired resolution and field of view. Furthermore, it is not practical to scan the tumor resection bed at different angles, nor does the instrumentation allow this. We hypothesized that a hand-held Raman spectrometer in conjunction with SERS nanoparticles could solve the issues related to acquisition speed and flexibility of the angle, leading to a viable technique for real-time guidance in the operating room. While several hand-held Raman scanners are available commercially, we deliberately chose a model that is already used in clinical trials,[33] albeit for the purpose of detecting "intrinsic" Raman tissue spectra. Intrinsic, *i.e.*, nonamplified conventional Raman spectroscopy has the disadvantage of requiring very long acquisition times in the order of 10−20 s per individual spectrum. Therefore, conventional intrinsic Raman spectroscopy is not expected to be useful for GBM resections in a clinical setting. Here we use the same hand-held scanner, however in conjunction with SERS nanoparticles that amplify the Raman signal by a factor of at least 10^8-fold. This allowed the recording of robust SERS nanoparticle spectra with acquisition times as short as 100 ms. We cross-validated the data acquired with the hand-held scanner using our static Raman microscope, and found the hand-held scanner to have three major advantages over the static Raman microscope: (1) It has the potential to be used in a clinical operating room. (2) It can probe areas of interest with near real-time imaging speed. (3) Most importantly, the surgeon can interrogate the operating bed with the hand-held probe from any desired angle, thereby providing optimal coverage of the tumor resection bed. This allows probing of the lateral walls of the resection bed that are usually hidden by overlying brain tissue when the fixed 90° angle Raman microscope is used.

In this study, those advantages translated into improved removal of residual tumor identified by microscopy during GBM surgery. The hand-held scanner was able to identify, in all 10 mice (n = 5 in group ii and iii each), small tumor foci that were not detected on the Raman images. This is attributable to the flexibility of angulating the hand-held scanner to probe any area in the operating bed, even those located at the lateral margins underneath overlying normal brain tissue. When resection was based on the hand-held scanner data alone, no residual tumor cells were found in the walls of the resection bed on histological analysis. This was achieved based on the SERS nanoparticle signal, without using any additional "safety margin". Safety margins are often used in current clinical practice in order to remove potentially present (but not confirmed) microscopic tumor extensions that cannot be visualized with the naked eye. However, safety margins have the disadvantage of increased patient morbidity due to unnecessary resection of adjacent healthy neurological structures. Remarkably, the hand-held Raman scanner also correctly identified the one

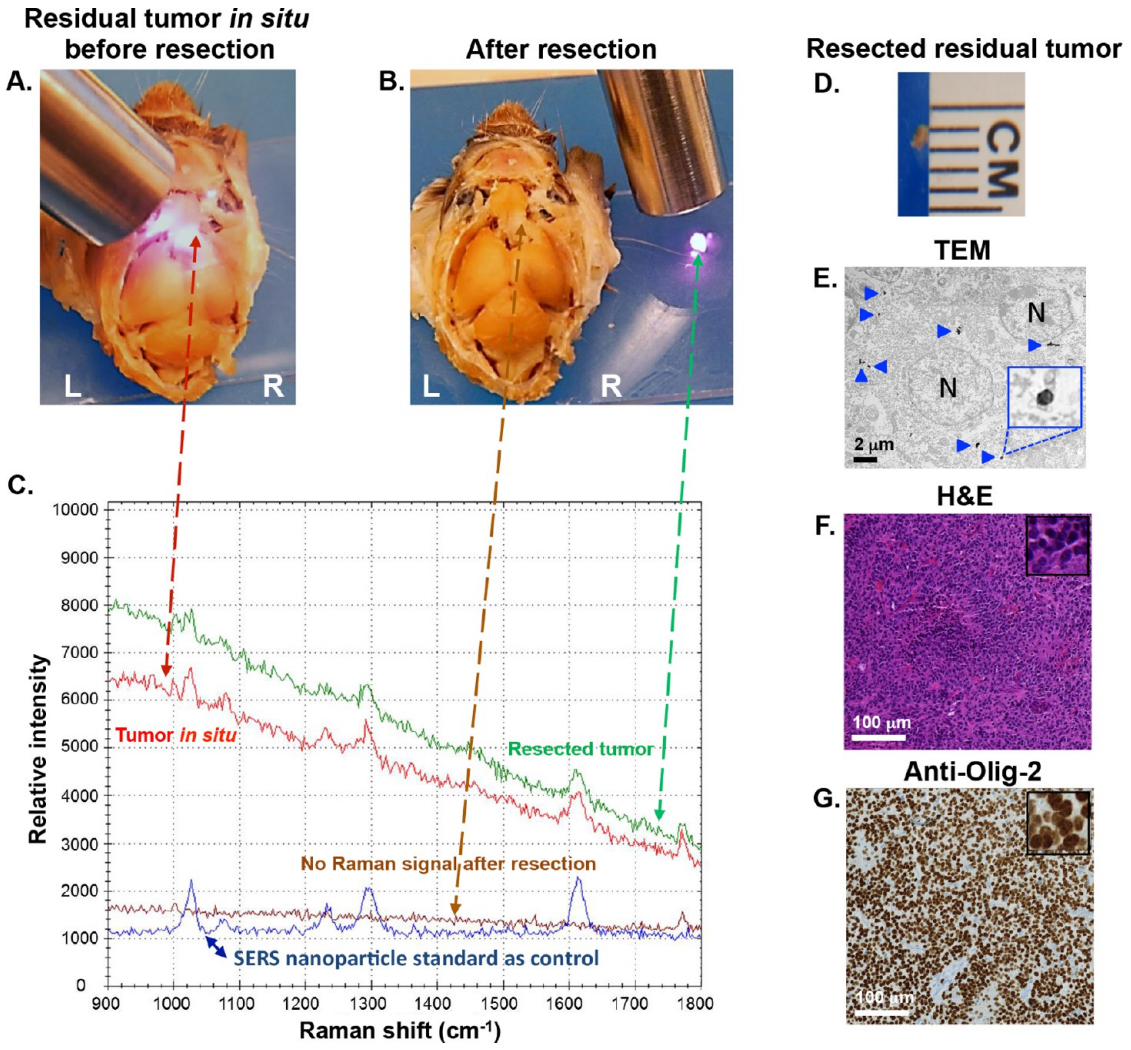

Figure 7. Representative example of tumor tissue detected only with the hand-held scanner. The tissue that was detected with the angulated hand-held Raman scanner (A) and subsequently resected (B and D) demonstrated the presence of the SERS nanoparticle Raman signature (C), that was confirmed to be tumor by transmission electron microscopy (TEM) and histology. TEM showed the presence of SERS nanoparticles within the resected specimen (E). H&E and immunohistochemical staining for tumor marker Olig-2 confirmed that the resected tissue indeed represented microscopic GBM cancer spread (F and G).

case where, unexpectedly, intraventricular tumor spread was present.

There are several possible explanations why the detection of GBMs with SERS nanoparticles is so robust, and results in the detection of microscopic tumor foci. We have previously shown in other mouse models of GBM that SERS nanoparticles can be found in infiltrating tumor zones, in microscopic fingerlike protrusions and in satellite lesions at or beyond the macroscopic tumor margin.[14] It is known that nanoparticles within a certain size range and surface charge accumulate specifically in cancer tissue, but not in normal tissues because of mechanisms unique to tumor biology. These mechanisms are described by the term EPR effect.[41−44] However, the mechanism of uptake of nanoparticles is in all likelihood not limited to the EPR effect. There are other more recently discovered mechanisms that contribute to nanoparticle uptake and retention in tumors, such as macropinocytosis.[45,46] Very recently, another previously unknown mechanism of nanoparticle delivery to tumors has been described: circulating white blood cells, especially monocytes, can take up nanoparticles while they circulate through blood vessels, and subsequently home to tumors.[47] This is important because cellular migration across the blood-brain-barrier is a known phenomenon.[48] Such a "trojan-horse" transport within transmigrating white blood cells[47] could explain the passage of nanoparticles across an intact blood-brain-barrier.

One of the limitations of our study is that we performed the tumor resections on brains that had been fixed in paraformaldehyde, and is therefore not fully representative of the actual surgical environment. We chose an *ex vivo* surgical approach in order to achieve the highest possible accuracy in correlating the Raman data with the histological data. Although surgery performed on brain tumors in living subjects is more complex, we do not foresee problems related to

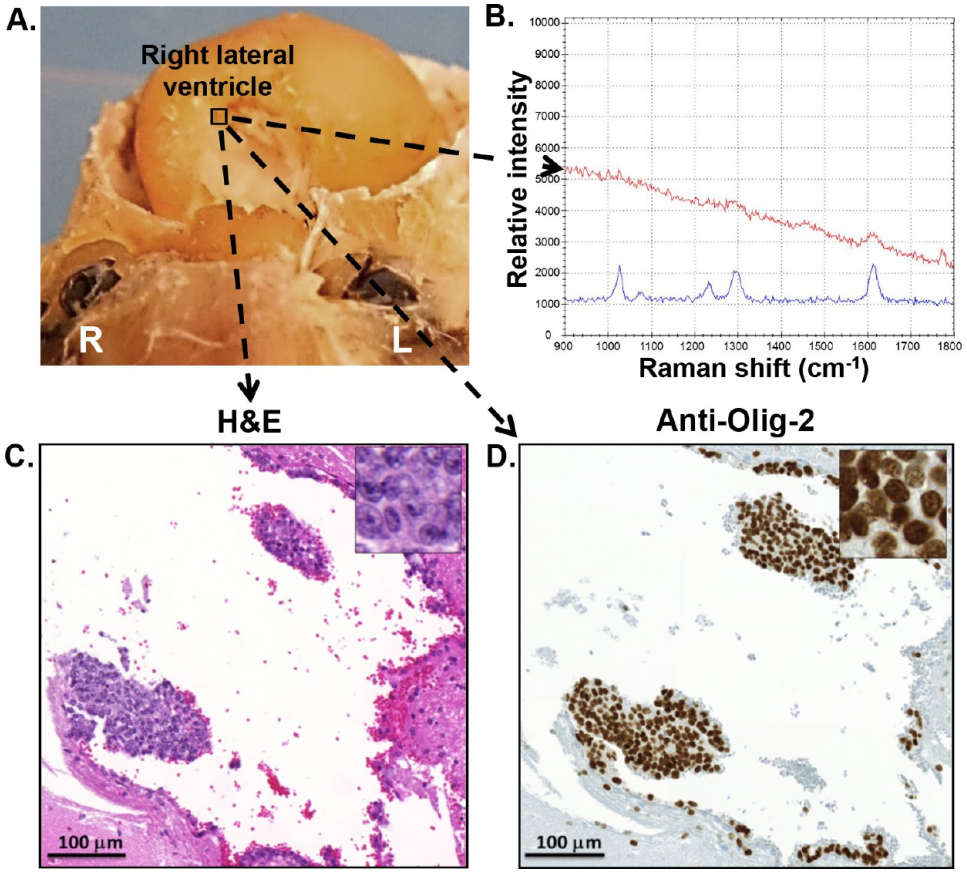

Figure 8. Detection of intraventricular tumor spread by hand-held Raman scanning. (A) Photograph showing an anterior view of the brain after complete resection guided by the hand-held Raman scanner. (B) SERS nanoparticle spectrum (red) from scanning the right ventricle for 2 s with 100% laser power at an acute angle (blue spectrum = SERS nanoparticle standard as control). (C and D) Histology of axial brain sections stained with H&E and anti-Olig-2 showing clusters of tumor cells within the ventricular system. Insets are 4× magnification.

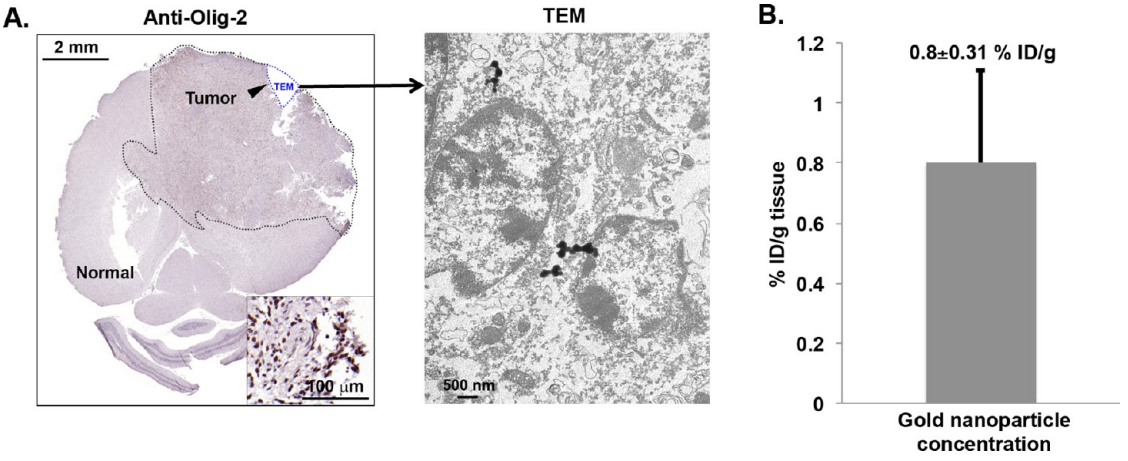

Figure 9. Validation of SERS nanoparticle accumulation within GBM tumors. (A) Immunohistochemistry (anti-Olig-2 antibody) and representative TEM image showing the presence of SERS nanoparticles within the tumor. The area labeled "TEM" on the IHC slice represents the tissue that was excised and processed for TEM imaging. (B) Quantification of SERS nanoparticle uptake within GBM tumor tissue *via* ICP-MS. Data represent mean ± SEM (n = 3 mice).

imaging agent extravasation in the operating bed due to bleeding. Another potential limitation of the technique is that depth penetration with conventional Raman spectroscopy imaging techniques is in the order of 5−7 mm.[14]

A hand-held Raman scanner in conjunction with highly sensitive SERS nanoparticles such as those used here can serve as a near real-time intraoperative scanning tool. It provides the capability of scanning the operative bed from any desired angle in order to

examine every aspect of the tumor bed. It therefore has the potential to replace other much more costly and time-consuming methods of intraoperative image-guidance (such as MRI), while at the same time delivering higher precision information about the actual location of brain tumor cell clusters. Studies examining patterns of brain tumor recurrence have consistently shown that 80−90% of recurrences are within the original treatment field, implicating residual tumor cells due to incomplete resection as the cause.[9,10] The ability to detect and resect microscopic tumor remnants could result in more complete tumor resections and potentially increase patient survival. A potential limitation toward this goal could be that even though the technique presented here may allow for complete tumor resections to be performed in principle, a truly complete removal of all tumor cells may be prohibitive in many patients because the tumor has spread to crucial neurological structures. It will require clinical studies to determine the benefit of brain tumor resections using SERS nanoparticle guidance. The more complete tumor resections achieved with this technique are expected to increase patient survival, but a potential increase in patient morbidity due to the increased amount of resected brain tissue will have to be evaluated. Other advantages of the presented method could be that operating times can be decreased markedly compared to the use of intraoperative MRI. Given that the SERS nanoparticles used here have already passed extensive cytotoxicity studies,[32] and the hand-held scanner used here has already been employed in clinical trials,[33] this SERS nanoparticle molecular imaging-guided surgical approach holds promise for clinical translation.

CONCLUSIONS

The potential of gold−silica SERS nanoparticles combined with a hand-held Raman scanner to provide image-guided surgical resection of GBMs is demonstrated in a transgenic murine model that closely recapitulates human brain tumors. Cross-validation with a conventional Raman microscope showed that both methods enabled equally sensitive Raman spectroscopic detection of SERS nanoparticles. While current generations of hand-held scanners are not yet able to routinely acquire entire SERS images, they have important advantages that are complementary and additive to SERS imaging instruments: first, their form factor allowing their use in the operating room; second, rapid scanning speed afforded by the SERS amplification, allowing near real-time scanning; and third, flexibility to probe any area of the operative bed due to variable tilt angles. We suggest that SERS-nanoparticle-guided surgery using hand-held Raman detectors represents a highly translatable approach to facilitate the resection of brain tumors and potentially other cancer types.

METHODS

SERS Nanoparticle Preparation. SERS nanoparticles (S420; Cabot, Boston, MA) are composed of spherical gold cores of approximately 60 nm in diameter and are coated with a monolayer of the Raman reporter 4,4′-dipyridyl and encapsulated in a silica shell of approximately 30 nm radius (total particle size ∼120 nm). For intravenous (iv) injections, particle concentrations were adjusted to 28.0 nM as determined by nanoparticle tracking analysis (NTA) using the Nanosight NS500 (Malvern, Worcestershire, U.K.), then suspended in 2-(*N*-morpholino)ethanesulfonic acid (MES) buffer (pH 7.3).

Generation of RCAS/tv-a Mouse GBM Model. All animal experiments were approved by the Institutional Animal Care and Use Committees of Memorial Sloan Kettering Cancer Center. We used a genetically engineered glioblastoma mouse model, PDGF-driven gliomas using RCAS/tv-a,[34,49] which is known to mimic the biology of human glioblastomas very closely.[35−37]

DF-1 cells were purchased from ATCC (Manassas, VA). Cells were grown at 39 °C according to ATCC instructions. Transfections were performed using Fugene 6 transfection kit (Roche # 11814443001, Indianapolis, IN) according to the manufacturer's instructions. The 4−6 week-old *nestin-tv-a/ink4a-arf−/−/pten*$^{fl/fl}$ mice were anesthetized with ketamine (0.1 mg/g) and xylazine (0.02 mg/g) and injected using stereotactic fixation device (Stoelting, Wood Dale, IL). One microliter of RCAS-PDGF-B or 1:1 mixture of 4 × 10^4 RCAS-PDGF-B and RCAS-Cre transfected DF-1 cells was delivered using a 30-gauge needle attached to a Hamilton syringe. Injections were targeted to the subventricular zone, coordinates bregma 1.7 mm (anterior), Lat −0.5 mm (right), and depth 2.5 mm from the dural surface.

Presurgical MRI. Four weeks after injection of the DF-1 cells, mice were imaged with MRI to determine tumor size and location for presurgical planning. MRI scans were conducted with a dedicated small animal MRI scanner consisting of a 4.7 T superconducting magnet (Bruker Biospin Corp., Billerica, MA), gradient (Resonance Research, Inc., Billerica, MA) with clear bore size of 20 cm, maximum gradient amplitude of 400 mT/m and maximum slew rate of 1300 T/(m/s) and a Bruker Avance electronics and console and IECO amplifiers (International Electric Co., Helsinki, Finland). Custom-made RF coils were used for RF excitation and detection during scanning. T2-weighted fast spin echo sequences (TE/TR 50 ms/2000 ms) were employed using 4 NEX, a 256 × 128 matrix, a 3.0 cm field-of-view, a slice thickness of 1000 μm and a total imaging time of ∼10 min.

Presurgical Preparation. The GBM bearing mice were generally sacrificed approximately 24 h after a single intravenous tail vein injection with SERS nanoparticles. Blood was collected *via* cardiac puncture, and Raman scans of the blood were obtained to verify that no residual SERS nanoparticles were present in the circulation. A craniotomy was performed to expose the brain, and brains intact within the skull bases were fixed in 4% paraformaldehyde for 24 h at 4 °C, followed by a rinse with PBS for 15−30 min and in 70% ethanol for another 24 h. Brains were scanned using the Raman microscope and the hand-held scanner before every tumor resection step as described below.

SERS Imaging Using the Raman Microscope. To acquire SERS images of the SERS nanoparticle distribution, we used a customized benchtop InVia Raman microscope (Renishaw, Gloucestershire, U.K.) equipped with a StreamLine Plus rapid imaging upgrade, piezo-controlled stage for micron-resolved spatial mapping, and a charge-coupled device detector with 1024 pixels (pixel size: 26 μm), spectral dispersion 1.25 cm^{-1}/pixel and spectral resolution of ∼3.7 cm^{-1}. We used a semiconductor diode near-infrared laser operating at 785 nm as the excitation source with a laser power output of ∼300 mW, resulting in approximately 100 mW at the skin surface. Raman images were acquired in the streamline scanning mode, using a computer-controlled *x*−*y* translation stage, an integration time of 2 s, a 5× lens (Leica,

Buffalo Grove, IL), 100 μm step size, and 100% laser power. Raman spectra were analyzed with Wire 3.4 Software (Renishaw).

SERS Detection Using the Hand-Held Raman Scanner. We used the MiniRam Raman hand-held scanner (B&W TEK, Inc., Newark, DE) with a 785 nm excitation laser. Raman spectra were analyzed with B&WSpec 4.01.26 Software (B&W TEK). For brain scanning, acquisition times of 1−2 s were used. First, scanning was performed by the neurosurgeon with the hand-held probe in its stand (delivered by B&W Tek together with the probe), which results in a fixed 90° angle. Subsequently, the probe was removed from the stand and variable angle scanning was performed, in order to simulate the actual clinical scenario. Holding the probe in his hands, the neurosurgeon carefully performed raster-scanning of the resection bed, at the optimal focal distance of approximately 5 mm from the tissue of interest.

Histological Analysis. Brain tissues after tumor resections were embedded in paraffin. Hematoxylin and eosin staining and immunohistochemistry (IHC) staining were performed on 5 μm-thick sections. The Discovery XT biomarker platform (Ventana, Tucson, AZ) was used for IHC staining of Olig2. Antigen was retrieved using the heat-induced antigen unmasking technique in citrate-based buffer (pH 6.0). Anti-Olig-2 (1:300, AB9610, Millipore, Temecula, CA) and biotin-labeled anti-rabbit antibody (1:300, BA-1000, Vector Laboratories, Burlingame, CA) were used as the primary and secondary antibodies, respectively. Streptavidin−biotin peroxidase was visualized by the Discovery DAB map detection kit (760-124, Ventana).

Procedure for TEM Brain Tissue Sample Preparation. Brain tissue samples were fixed in 2.5% glutaraldehyde/2% paraformaldehyde in cacodylate buffer, rinsed in buffer and post fixed in 2% osmium tetroxide for 1 h. The samples ware rinsed in double distilled water, followed by a graded series of aqueous ethanol solutions (50%, 75%, 95% to 100% alcohol), followed by propylene oxide, and overnight 1:1 propylene oxide/PolyBed 812. The samples were embedded in Poly/Bed 812 and cured in a 60 °C oven. Ultrathin sections were obtained with a Reichert Ultracut S microtome. Sections were stained with uranyl acetate and lead citrate and photographed using a Jeol 1200EX transmission electron microscope.

Inductively Coupled Plasma Mass Spectrometry (ICP-MS). Brain tumor tissue samples of known masses were taken up in 2 mL of freshly prepared *aqua regia* (1:3 ratio of concentrated nitric acid and hydrochloric acid) and heated to dryness. This process was repeated until the samples could fully dissolve in the acidic solution. The samples were then dissolved in 0.5 mL of *aqua regia* and subsequently diluted with water to 7.5 mL. The samples were then analyzed at the Brooklyn College Environmental Sciences Analytical Center on a PerkinElmer Elan DRC-e ICP-MS instrument and referenced to a HAuCl4-derived calibration curve.

Conflict of Interest: The authors declare no competing financial interest.

Supporting Information Available: (i) Resection without Raman guidance including Figure S1. This material is available free of charge *via* the Internet at http://pubs.acs.org.

Acknowledgment. We would like to thank Ronald Blasberg, M.D. for critical review of the manuscript and many helpful suggestions. We also thank Leila Akkari, Ph.D. and Johanna Joyce, Ph.D. for providing us with additional RCAS/tv-a mice; Volker Neuschmelting, M.D. for critical review of the manuscript; the MSKCC electron microscopy core, molecular cytology core and small animal imaging core facilities; and the Brooklyn College Environmental Sciences Analytical Center where the ICP-MS studies were performed. We acknowledge the following grant support: NIH R01 EB017748 (M.F.K.); NIH K08 CA16396 (M.F.K.); M.F.K. is a Damon Runyon-Rachleff Innovator supported (in part) by the Damon Runyon Cancer Research Foundation (DRR-29-14); MSKCC Center for Molecular Imaging and Nanotechnology Grant (M.F.K.); MSKCC Technology Development Grant (M.F.K.); Geoffrey Beene Cancer Research Center at MSKCC Grant Award (M.F.K.) and Shared Resources Award (M.F.K.); The Dana Foundation Brain and Immuno-Imaging Grant (M.F.K.); Dana Neuroscience Scholar Award (M.F.K.); Bayer HealthCare Pharmaceuticals/RSNA Research Scholar Grant (M.F.K.); MSKCC Brain Tumor Center Grant (M.F.K.); Society of MSKCC Research Grant (M.F.K.); and R25T Molecular Imaging for Training in Oncology Program (2R25-CA096945; principal investigator H. Hricak; fellow: J.M.S.) from the US National Cancer Institute. Acknowledgments are also extended to the grant-funding support provided by the MSKCC NIH Core Grant (P30-CA008748).

REFERENCES AND NOTES

1. Adamson, C.; Kanu, O. O.; Mehta, A. I.; Di, C.; Lin, N.; Mattox, A. K.; Bigner, D. D. Glioblastoma Multiforme: A Review of Where We Have Been and Where We Are Going. *Expert Opin. Invest. Drugs* **2009**, *18*, 1061–1083.
2. Hoover, J. M.; Chang, S. M.; Parney, I. F. Clinical Trials in Brain Tumor Surgery. *Neuroimaging Clin. N. Am.* **2010**, *20*, 409–424.
3. Bucci, M. K.; Maity, A.; Janss, A. J.; Belasco, J. B.; Fisher, M. J.; Tochner, Z. A.; Rorke, L.; Sutton, L. N.; Phillips, P. C.; Shu, H. K. Near Complete Surgical Resection Predicts a Favorable Outcome in Pediatric Patients with Nonbrainstem, Malignant Gliomas: Results from a Single Center in the Magnetic Resonance Imaging Era. *Cancer* **2004**, *101*, 817–824.
4. Ngwenya, L. B.; Chiocca, E. A. Extent of Resection. *J. Neurosurg.* **2011**, *115*, 1–2discussion 2.
5. Stupp, R.; Hegi, M. E.; van den Bent, M. J.; Mason, W. P.; Weller, M.; Mirimanoff, R. O.; Cairncross, J. G.; European Organisation for Research and Treatment of Cancer Brain Tumor and Radiotherapy Groups; *et al.* Changing Paradigms—An Update on the Multidisciplinary Management of Malignant Glioma. *Oncologist* **2006**, *11*, 165–180.
6. Rogers, L.; Pueschel, J.; Spetzler, R.; Shapiro, W.; Coons, S.; Thomas, T.; Speiser, B. Is Gross-Total Resection Sufficient Treatment for Posterior Fossa Ependymomas?. *J. Neurosurg.* **2005**, *102*, 629–636.
7. Sanai, N.; Polley, M. Y.; McDermott, M. W.; Parsa, A. T.; Berger, M. S. An Extent of Resection Threshold for Newly Diagnosed Glioblastomas. *J. Neurosurg.* **2011**, *115*, 3–8.
8. Bloch, O.; Han, S. J.; Cha, S.; Sun, M. Z.; Aghi, M. K.; McDermott, M. W.; Berger, M. S.; Parsa, A. T. Impact of Extent of Resection for Recurrent Glioblastoma on Overall Survival: Clinical Article. *J. Neurosurg.* **2012**, *117*, 1032–1038.
9. Petrecca, K.; Guiot, M. C.; Panet-Raymond, V.; Souhami, L. Failure Pattern Following Complete Resection plus Radiotherapy and Temozolomide is at the Resection Margin in Patients with Glioblastoma. *J. Neurooncol.* **2013**, *111*, 19–23.
10. Oh, J.; Sahgal, A.; Sanghera, P.; Tsao, M. N.; Davey, P.; Lam, K.; Symons, S.; Aviv, R.; Perry, J. R. Glioblastoma: Patterns of Recurrence and Efficacy of Salvage Treatments. *Can. J. Neurol. Sci.* **2011**, *38*, 621–625.
11. Toms, S. A.; Lin, W. C.; Weil, R. J.; Johnson, M. D.; Jansen, E. D.; Mahadevan-Jansen, A. Intraoperative Optical Spectroscopy Identifies Infiltrating Glioma Margins with High Sensitivity. *Neurosurgery* **2005**, *57*, 382–391.
12. Albert, F. K.; Forsting, M.; Sartor, K.; Adams, H. P.; Kunze, S. Early Postoperative Magnetic Resonance Imaging After Resection of Malignant Glioma: Objective Evaluation of Residual Tumor and Its Influence on Regrowth and Prognosis. *Neurosurgery* **1994**, *34*, 45–60;discussion 60−41.
13. Siomin, V.; Barnett, G. Intraoperative Imaging in Glioblastoma Resection. *Cancer J.* **2003**, *9*, 91–98.
14. Kircher, M. F.; de la Zerda, A.; Jokerst, J. V.; Zavaleta, C. L.; Kempen, P. J.; Mittra, E.; Pitter, K.; Huang, R.; Campos, C.; Habte, F.; *et al.* A Brain Tumor Molecular Imaging Strategy Using a New Triple-Modality MRI-Photoacoustic-Raman Nanoparticle. *Nat. Med.* **2012**, *18*, 829–834.
15. Orringer, D. A.; Chen, T.; Huang, D. L.; Armstead, W. M.; Hoff, B. A.; Koo, Y. E.; Keep, R. F.; Philbert, M. A.; Kopelman, R.; Sagher, O. The Brain Tumor Window Model: A Combined Cranial Window and Implanted Glioma Model for Evaluating Intraoperative Contrast Agents. *Neurosurgery* **2010**, *66*, 736–743.

16. Gerstner, E. R.; Chen, P. J.; Wen, P. Y.; Jain, R. K.; Batchelor, T. T.; Sorensen, G. Infiltrative Patterns of Glioblastoma Spread Detected *via* Diffusion MRI After Treatment with Cediranib. *Neuro-Oncol.* **2010**, *12*, 466–472.
17. de Groot, J. F.; Fuller, G.; Kumar, A. J.; Piao, Y.; Eterovic, K.; Ji, Y.; Conrad, C. A. Tumor Invasion after Treatment of Glioblastoma with Bevacizumab: Radiographic and Pathologic Correlationin Humans and Mice. *Neuro-Oncol.* **2010**, *12*, 233–242.
18. Reinges, M. H.; Nguyen, H. H.; Krings, T.; Hutter, B. O.; Rohde, V.; Gilsbach, J. M. Course of Brain Shift During Microsurgical Resection of Supratentorial Cerebral Lesions: Limits of Conventional Neuronavigation. *Acta Neurochir (Wien)* **2004**, *146*, 369–377;discussion 377.
19. Ludemann, L.; Hamm, B.; Zimmer, C. Pharmacokinetic Analysis of Glioma Compartments with Dynamic Gd-DTPA-Enhanced Magnetic Resonance Imaging. *Magn. Reson. Imaging* **2000**, *18*, 1201–1214.
20. Knauth, M.; Aras, N.; Wirtz, C. R.; Dorfler, A.; Engelhorn, T.; Sartor, K. Surgically Induced Intracranial Contrast Enhancement: Potential Source of Diagnostic Error in Intraoperative MR Imaging. *AJNR Am. J. Neuroradiol.* **1999**, *20*, 1547–1553.
21. Pronin, I. N.; McManus, K. A.; Holodny, A. I.; Peck, K. K.; Kornienko, V. N. Quantification of Dispersion of Gd-DTPA from the Initial Area of Enhancement into the Peritumoral Zone of Edema in Brain Tumors. *J. Neurooncol.* **2009**, *94*, 399–408.
22. Saether, C. A.; Torsteinsen, M.; Torp, S. H.; Sundstrom, S.; Unsgard, G.; Solheim, O. Did Survival Improve After the Implementation of Intraoperative Neuronavigation and 3D Ultrasound in Glioblastoma Surgery? A Retrospective Analysis of 192 Primary Operations. *J. Neurol. Surg. A Cent. Eur. Neurosurg.* **2012**, *73*, 73–78.
23. Ulrich, N. H.; Burkhardt, J. K.; Serra, C.; Bernays, R. L.; Bozinov, O. Resection of Pediatric Intracerebral Tumors with the Aid of Intraoperative Real-Time 3-D Ultrasound. *Childs Nerv. Syst.* **2012**, *28*, 101–109.
24. Beljebbar, A.; Dukic, S.; Amharref, N.; Manfait, M. Ex vivo and in vivo Diagnosis of C6 Glioblastoma Development by Raman Spectroscopy Coupled to a Microprobe. *Anal. Bioanal. Chem.* **2010**, *398*, 477–487.
25. Ji, M.; Orringer, D. A.; Freudiger, C. W.; Ramkissoon, S.; Liu, X.; Lau, D.; Golby, A. J.; Norton, I.; Hayashi, M.; Agar, N. Y.; *et al.* Rapid, Label-Free Detection of Brain Tumors with Stimulated Raman Scattering Microscopy. *Sci. Transl. Med.* **2013**, *5*, 201ra119.
26. Ozawa, T.; Britz, G. W.; Kinder, D. H.; Spence, A. M.; VandenBerg, S.; Lamborn, K. R.; Deen, D. F.; Berger, M. S. Bromophenol Blue Staining of Tumors in a Rat Glioma Model. *Neurosurgery* **2005**, *57*, 1041–1047discussion 1041−1047.
27. Shinoda, J.; Yano, H.; Yoshimura, S.; Okumura, A.; Kaku, Y.; Iwama, T.; Sakai, N. Fluorescence-Guided Resection of Glioblastoma Multiforme by Using High-Dose Fluorescein Sodium. Technical Note. *J. Neurosurg.* **2003**, *99*, 597–603.
28. Stummer, W.; Pichlmeier, U.; Meinel, T.; Wiestler, O. D.; Zanella, F.; Reulen, H. J.; Group, A. L.-G. S. Fluorescence-Guided Surgery with 5-Aminolevulinic Acid for Resection of Malignant Glioma: A Randomised Controlled Multicentre Phase III Trial. *Lancet Oncol.* **2006**, *7*, 392–401.
29. Huang, R.; Vider, J.; Kovar, J. L.; Olive, D. M.; Mellinghoff, I. K.; Mayer-Kuckuk, P.; Kircher, M. F.; Blasberg, R. G. Integrin $\alpha v\beta 3$-Targeted IRdye 800CW Near-Infrared Imaging of Glioblastoma. *Clin. Cancer Res.* **2012**, *18*, 5731–5740.
30. Kantelhardt, S. R.; Diddens, H.; Leppert, J.; Rohde, V.; Huttmann, G.; Giese, A. Multiphoton Excitation Fluorescence Microscopy of 5-Aminolevulinic Acid Induced Fluorescence in Experimental Gliomas. *Lasers Surg. Med.* **2008**, *40*, 273–281.
31. de la Zerda, A.; Bodapati, S.; Teed, R.; Schipper, M. L.; Keren, S.; Smith, B. R.; Ng, J. S.; Gambhir, S. S. A Comparison Between Time Domain and Spectral Imaging Systems for Imaging Quantum Dots in Small Living Animals. *Mol. Imaging Biol.* **2010**, *12*, 500–508.
32. Thakor, A. S.; Luong, R.; Paulmurugan, R.; Lin, F. I.; Kempen, P.; Zavaleta, C.; Chu, P.; Massoud, T. F.; Sinclair, R.; Gambhir, S. S. The Fate and Toxicity of Raman-Active Silica-Gold Nanoparticles in Mice. *Sci. Transl. Med.* **2011**, *3*, 79ra33.
33. Horsnell, J.; Stonelake, P.; Christie-Brown, J.; Shetty, G.; Hutchings, J.; Kendall, C.; Stone, N. Raman Spectroscopy--A New Method for the Intra-Operative Assessment of Axillary Lymph Nodes. *Analyst* **2010**, *135*, 3042–3047.
34. Hambardzumyan, D.; Amankulor, N. M.; Helmy, K. Y.; Becher, O. J.; Holland, E. C. Modeling Adult Gliomas Using RCAS/t-va Technology. *Transl. Oncol* **2009**, *2*, 89–95.
35. Brennan, C.; Momota, H.; Hambardzumyan, D.; Ozawa, T.; Tandon, A.; Pedraza, A.; Holland, E. Glioblastoma Subclasses Can Be Defined by Activity Among Signal Transduction Pathways and Associated Genomic Alterations. *PLoS One* **2009**, *4*, e7752.
36. Dougherty, J. D.; Fomchenko, E. I.; Akuffo, A. A.; Schmidt, E.; Helmy, K. Y.; Bazzoli, E.; Brennan, C. W.; Holland, E. C.; Milosevic, A. Candidate Pathways for Promoting Differentiation or Quiescence of Oligodendrocyte Progenitor-Like Cells in Glioma. *Cancer Res.* **2012**, *72*, 4856–4868.
37. Verhaak, R. G.; Hoadley, K. A.; Purdom, E.; Wang, V.; Qi, Y.; Wilkerson, M. D.; Miller, C. R.; Ding, L.; Golub, T.; Mesirov, J. P.; *et al.* Integrated Genomic Analysis Identifies Clinically Relevant Subtypes of Glioblastoma Characterized by Abnormalities in PDGFRA, IDH1, EGFR, and NF1. *Cancer Cell* **2010**, *17*, 98–110.
38. Zavaleta, C. L.; Kircher, M. F.; Gambhir, S. S. Raman's "Effect" on Molecular Imaging. *J. Nucl. Med.* **2011**, *52*, 1839–1844.
39. Pfister, S.; Witt, O. Pediatric Gliomas. *Recent Results Cancer Res.* **2009**, *171*, 67–81.
40. Pollack, I. F. Brain Tumors in Children. *N. Engl. J. Med.* **1994**, *331*, 1500–1507.
41. Maeda, H. The Link Between Infection and Cancer: Tumor Vasculature, Free Radicals, and Drug Delivery to Tumors *via* the EPR Effect. *Cancer Sci.* **2013**, *104*, 779–789.
42. Maeda, H.; Nakamura, H.; Fang, J. The EPR Effect for Macromolecular Drug Delivery to Solid Tumors: Improvement of Tumor Uptake, Lowering of Systemic Toxicity, and Distinct Tumor Imaging in vivo. *Adv. Drug Delivery Rev.* **2013**, *65*, 71–79.
43. Matsumura, Y.; Maeda, H. A New Concept for Macromolecular Therapeutics in Cancer Chemotherapy: Mechanism of Tumoritropic Accumulation of Proteins and the Antitumor Agent Smancs. *Cancer Res.* **1986**, *46*, 6387–6392.
44. Thakor, A. S.; Gambhir, S. S. Nanooncology: The Future of Cancer Diagnosis and Therapy. *CA Cancer J. Clin.* **2013**, *63*, 395–418.
45. Fincham, V. J.; Unlu, M.; Brunton, V. G.; Pitts, J. D.; Wyke, J. A.; Frame, M. C. Translocation of Src Kinase to the Cell Periphery Is Mediated by the Actin Cytoskeleton Under the Control of the Rho Family of Small G Proteins. *J. Cell Biol.* **1996**, *135*, 1551–1564.
46. Weissleder, R.; Nahrendorf, M.; Pittet, M. J. Imaging Macrophages with Nanoparticles. *Nat. Mater.* **2014**, *13*, 125–138.
47. Smith, B. R.; Ghosn, E. E.; Rallapalli, H.; Prescher, J. A.; Larson, T.; Herzenberg, L. A.; Gambhir, S. S. Selective Uptake of Single-Walled Carbon Nanotubes by Circulating Monocytes for Enhanced Tumour Delivery. *Nat. Nanotechnol.* **2014**, *9*, 481–487.
48. Engelhardt, B.; Ransohoff, R. M. Capture, Crawl, Cross: The T Cell Code to Breach the Blood-Brain Barriers. *Trends Immunol.* **2012**, *33*, 579–589.
49. Pitter, K. L.; Galban, C. J.; Galban, S.; Tehrani, O. S.; Li, F.; Charles, N.; Bradbury, M. S.; Becher, O. J.; Chenevert, T. L.; Rehemtulla, A.; *et al.* Perifosine and CCI 779 Co-Operate to Induce Cell Death and Decrease Proliferation in PTEN-Intact and PTEN-Deficient PDGF-Driven Murine Glioblastoma. *PLoS One* **2011**, *6*, e14545.